Article

Journal of
Biomedical Nanotechnology
Vol. 10, 405–414, 2014
www.aspbs.com/jbn

Anomalous Subsurface Thermal Behavior in Tissue Mimics Upon Near Infrared Irradiation Mediated Photothermal Therapy

Soham Ghosh[1], Nilamani Sahoo[1], P. R. Sajanlal[2], Nirod Kumar Sarangi[2], Nivarthi Ramesh[2], Tapobrata Panda[3], T. Pradeep[2], and Sarit Kumar Das[1,*]

[1] *Department of Mechanical Engineering, Indian Institute of Technology Madras, Chennai 600036, India*
[2] *Department of Chemistry, Indian Institute of Technology Madras, Chennai 600036, India*
[3] *Biochemical Engineering Laboratory, Indian Institute of Technology Madras, Chennai 600036, India*

Photothermal therapy using (Near Infrared) NIR region of EM spectrum is a fast emerging technology for cancer therapy. Different types of nanoparticles may be used for enhancing the treatment. Though the treatment protocols are developed based on experience driven estimated temperature increase in the tissue, it is not really known what spatiotemporal thermal behavior in the tissue is. In this work, this thermal behavior of tissue models is investigated with and without using nanoparticles. An increased temperature inside tissue compared to surface is observed which is counter intuitive from the present state of knowledge. It is shown from fiber level microstructure that this increased temperature leads to enhanced damage at the deeper parts of biomaterials. Nanoparticles can be utilized to control this temperature increase spatially. A multiple scattering based physical model is proposed to explain this counterintuitive temperature rise inside tissue. The results show promising future for better understanding and standardizing the protocols for photothermal therapy.

KEYWORDS: *Photothermal Therapy, Tissue Mimics, Plasmonic Nanomaterial, Collagen Denaturation, Mathematical Model.*

INTRODUCTION

The near infrared (NIR) spectral region of 750–1100 nm has the highest physiological transmission and is also a premier optical communication gateway into the human body.[1] The absence of strong intrinsic chromophores responsible for strong absorbance at this spectral range is the reason behind this selective behavior of tissues. This spectral transparency is utilized in various clinical applications like optical imaging of internal organs[2] and treatment of malignant tumors using NIR lasers known as photothermal therapy.[3–5]

Application of NIR laser in photothermal therapy is often accompanied by usage of plasmonic nanoparticles. Plasmonic nanomaterials have been used for the past several years to develop ultrasensitive diagnostic,[6,7] spectroscopic[8,9] and therapeutic technologies[3,4,10,11] utilizing their electromagnetic properties. Tunable plasmonic nanomaterials have attracted immense attention for their enhanced optical absorption coefficients and reduced scattering coefficient which is desirable for minimum collateral damage of healthy tissues. They have potential as biocompatible nanoantennas for cancer treatment that locally convert NIR electromagnetic energy to thermal energy for tumor ablation.

The underlying mechanism in photothermal therapies is to cause thermal damages of various degrees (consisting of coagulation, vaporization, vacuolization, pyrolysis, and ablation) in the tissue. In clinical setting this therapy requires precise estimation of spatiotemporal temperature rise history in the tissue. The proper estimation of spatiotemporal temperature profile is required for two reasons, for complete ablation of necrotic tissue and for minimizing damage to the surrounding healthy tissue. Once the temperature is estimated the thermal damage can be quantified using Arrhenius type damage integral which is computed based on temporal thermal profile. Therefore quantification of thermal profile and resulting damage is an immensely important aspect of the treatment protocol to

*Author to whom correspondence should be addressed.
Email: skdas@iitm.ac.in
Received: 16 September 2012
Accepted: 6 May 2013

the oncosurgeons.[12,13] The damage optimization protocol to keep the complications minimal is often experiment and 'experience' based. Even in these experiments only surface temperature is measured transiently and the calculation of internal damage is carried out with an attenuating light propagation model coupled with heat transfer physics. The resulting spatial thermal distribution over time is considered to be adequate to calculate thermal damage of the tissues.

Several attempts have been reported to measure the surface temperature of tumors in the course of photothermal treatment using near infrared imaging and its prediction using mathematical models.[5,14,15] However, the knowledge about how NIR light actually interacts with tissue and what is the ultimate thermal fate of the tissues at depth because of this interaction, is still very limited. As the biological tissue is a particulate media, the behavior of light propagation in this system may not be purely attenuating as assumed in the present therapies. The existence of multiple scattering in tissue which is already confirmed in the context of tomography and spectroscopy may be dominant in the thermal realm as well. Thus we believe that it would not be a good assumption to stick to an assumed attenuating temperature profile inside tissue and calculate the damage accordingly, which may lead to erroneous therapeutic protocol.

In this paper, we quantified the actual spatiotemporal temperature generation inside biological systems using a model biomaterial widely used, collagen gel. Agar gel was also used as a second biomaterial. Without depending on surface temperature alone we have measured the temperature distribution in tissue mimics subjected to NIR irradiation to investigate the actual thermal history inside tissue. Based on our results we report the observation of a completely counterintuitive thermal profile in tissue mimics that shows a temperature maximum in the interior of the tissue compared to the surface in contrast to the expected monotonic decay of temperature in models based on surface temperature alone. To further extend the implication of this observation in photothermal therapy, the biomaterial was impregnated with two types of nanoparticles. On NIR laser irradiation, nanoparticle impregnated biomaterials also showed enhanced temperature inside but the temperature peak shifted towards the surface. To characterize the implication of this increased temperature inside biomaterials, we imaged the microstructural change of collagen fiber using atomic force microscopy. Interestingly it was observed that increasing temperature inside biomaterial correlates to considerable microstructural change compared to the surface. The consequence of this increased temperature and higher damage inside tissue compared to surface can be far reaching which is explained later. The physics behind the phenomenon of enhanced temperature inside tissue is revealed through multiple scattering and classical thermal transport in the context of photothermal therapy.

MATERIALS AND METHODS

Measurement of Temperature Inside Tissue Mimics

Experiments were designed to measure the temperature distribution inside tissue mimics upon NIR irradiation. Two biologically relevant systems and commonly used tissue mimics (collagen gel and agar) were heated using a NIR laser and the temperature rise was measured inside the gel matrices. *In vitro* experiments were performed in such a way to avoid multiple mutually interacting physiological effects. Another reason for *in vitro* measurement is that for temperature measurement, penetrating thermocouples can be used. For *in vivo* experiment thermocouples can not be inserted inside the tissue. Non penetrating probes can be used for *in vivo* applications but they are associated with high degree of error. As the temperature rise during photothermal therapy is not high, small errors are magnified to produce misleading result justifying the *in vitro* experiment with thermocouples. The experimental set-up (cf Fig. 1 and supplementary material Fig. S-1) consists of the test acrylic beaker which contains the biomaterial, used for the study. The beaker had 14 holes bored at 2.5 mm spacing and 1 mm *J* type sheathed thermocouples were inserted into each hole which can reach up to the long axis of the cylinder (refer to supplementary material Figs. S-2(a) and S-2(b)). There was an arrangement to move the thermocouples in radial direction as well. The total length over which the thermocouples were inserted was 3.5 cm. The temperature measurements had an uncertainty of 0.1 °C and the thermocouples were placed helically around the cylinder to ensure minimum interference between them and to prevent breakage of the acrylic beaker due to high stress generation during machining (Fig. S2-(b)). It was maintained that the topmost thermocouple tip was near to the surface but covered by the biomaterial. This way it was

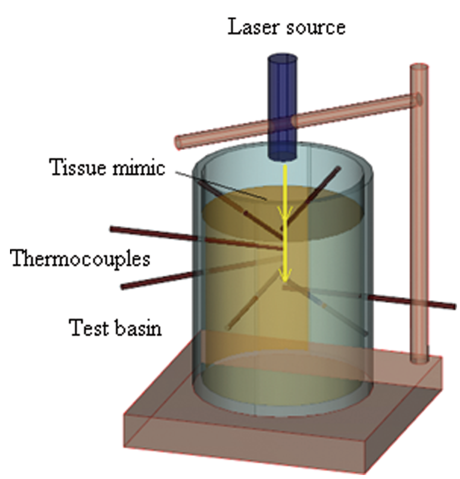

Figure 1. **Schematic diagram of experimental set-up. The thermocouples are inserted inside the test beaker and the outputs are connected to a data acquisition system. A continuous wave diode-pumped solid-state laser source (MONOPOWER™) of wavelength 1064 nm to irradiate the tissue mimic gel.**

ensured that the thermocouples were not directly heated by laser. The inner wall of the beaker was covered to arrest any leakage of biomaterials. A continuous wave diode-pumped solid-state laser source (MONOPOWER™-1064-500 MM, ALPHALAS GMBH, Gottingen, Germany) of 1064 nm wavelength was fixed vertically on the frame at a distance of 3.5 cm above the biomaterial surface to irradiate it. The laser was accompanied with a laser diode driver and Thermo-Electric Cooler (TEC) controller (LDD1-1T-D, ALPHALAS GMBH, Gottingen, Germany) to set and maintain the laser power. The laser power could be controlled to vary between 300 mW (power density or pd = 2.39 W/cm^2) to 600 mW (pd = 4.78 W/cm^2). The beam diameter at the biomaterial surface was 4 mm. The distance between the laser and the sample was fixed in all the measurements.

Materials for Synthesis of Nanostructures

Aniline from Sigma Aldrich, India was double distilled before use; ascorbic acid, silver nitrate, cetyltrimethylammonium bromide (CTAB), tetrachloroauric acid trihydrate and citric acid were procured from CDH, India. Highly purified distilled water was used throughout the experiment.

Synthesis of Gold Mesoflowers

The Au mesoflowers were synthesized as per our earlier procedure.[16] Briefly, 20 mL of CTAB (100 mM) was taken in a beaker and 335 μL of Au^{3+} (25 mM), 125 μL of $AgNO_3$ (10 mM) and 135 μL of ascorbic acid (100 mM) were added sequentially. To this solution, 4 mL of Au/oligoaniline nanoparticles synthesized as per our earlier report[17] was added and the solution was maintained at 80 °C for 1 h. It was then allowed to cool to room temperature. After 1 h, the solution was centrifuged at 3500 rpm for 4 min. The residue was washed with water three times in order to remove excess CTAB and other unwanted materials. The slight yellowish residue of Au MFs was redispersed in 20 mL of deionized water. This procedure yielded mesoflowers of size 0.5–1 μm. The prepared mesoflower solution showed an absorption peak around 1150 nm, which is closed to the wavelength of our laser i.e., 1064 nm.

Synthesis of Nearly Spherical Particles

For the synthesis of nearly spherical nanoparticles, 335 μL Au^{3+} (25 mM), 125 μL $AgNO_3$ (10 mM), and 135 μL freshly prepared ascorbic acid (100 mM) were added sequentially to 20 mL of CTAB (100 mM) solution taken in a beaker. To this growth solution 5 mL of Au/oligoaniline nanoparticles was added. The beaker was immediately placed in an ice bath and kept for 2 h. After 1 h, the solution was centrifuged at 5000 rpm for 5 min. The residue was washed with water three times to remove excess surfactants and was characterized. The as prepared spherical particles showed an absorption peak around 690 nm. The SEM image of synthesized nanoparticles are shown in Figures 2, S-3 and S-4.

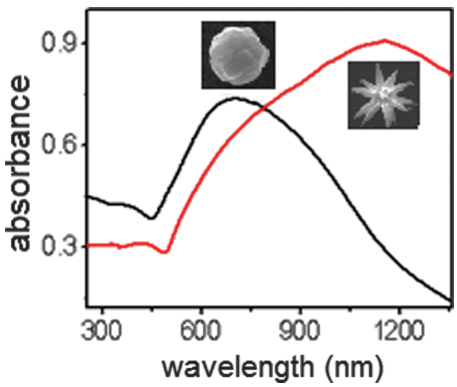

Figure 2. Absorption spectrum of gold mesoflower shows the maximum at around 1150 nm and that of nanosphere at 690 nm. Inset: Au Mα based EDAX image of a single gold mesoflower and nanosphere.

Preparation of Nanoparticle Embedded Agar Gel

Agar powder was purchased from Sisco Research Laboratories (Mumbai, India) and was tested for gelation at different concentrations. For an optimum mechanical and thermal property, the powder was mixed with water in 2% by weight. The mixture was heated till the murky solution becomes clear and boiling starts. The solution was continuously stirred to prevent burning of agar gel. Nanoparticle dispersion was sonicated for two hours. The agar solution was poured into the test container and after the gel becomes considerably viscous, the nanoparticle suspension was gently mixed into it. This is required to prevent the sedimentation of the heavy nanoparticles in the gel. Then it was kept in the room temperature for 1 hour for solidification.

Preparation of Nanoparticle Embedded Collagen Gel

Type I collagen from bovine tendon wet tissue (250 mg of pure collagen in 1 gm of wet tissue) was brought from Central Leather Research Laboratory, Chennai http://www.clri.org/. It was dissolved in 0.3 M acetic acid solution and the pH was set to 3.2. Then it was centrifuged at ice bath to get the required viscosity mimicking the animal tissue. The nanoparticles were sprinkled in the liquid solution and stirred for 8 hours to get a homogeneous nanoparticle embedded tissue.

Experimental Groups for Temperature Measurement

Experiments were performed without and with nanoparticles in both collagen gel and agar gel. In bare collagen gel (without nanoparticle), the experiments were performed at 4 power levels, 348 mW (pd = 2.77 W/cm^2), 446 mW

(pd = 3.55 W/cm^2), 502 mW (pd = 3.99 W/cm^2) and 558 mW (pd = 4.44 W/cm^2). The laser power density used in this study is of similar order of magnitude as practiced in clinical settings.[5] For experiments with nanoparticles, two types of nanoparticles were used, mesoflower and nanosphere at the concentration of 25 mg/ Kg of collagen gel, the laser power was maintained at 446 mW (pd = 3.55 W/cm^2). The effect of nanoparticle concentration in collagen gel was studied at 446 mW (pd = 3.55 W/cm^2) power for both nanoparticles. The concentrations were 25, 50 and 75 mg/Kg.

Atomic Force Microscopy

To characterize the thermal denaturation of the collagen gel upon NIR laser irradiation, atomic force microscopy was used. After conducting each laser irradiation experiment a 30 μL droplet of irradiated collagen gel was collected from three different depths (surface, depth of maximum temperature, 2 mm beyond maximum temperature) was smeared and fixed on a glass slide for imaging. The imaging was performed on an XE-100 AFM (Park Systems, Singapore). Non contact mode was used for imaging with ACTA probes supplied by Forevision Instrument's (I) Pvt. Ltd., Hyderabad, India. This silicon made probe had a radius of curvature < 10 nm and force constant of 40 N/m. A scanner of 5 μm $\times$ 5 μm size was used with a typical scan rate of 1 Hz.

Statistical Analysis

Each experimental group was performed at least three times ($n \geq 3$). The results are presented as mean $\pm$ standard deviation around mean. The student t-test was performed for comparing two groups at 95% confidence level.

Modeling for Increased Light Intensity Inside Biomaterials

The models used so far to find laser interaction in biological systems use inherent attenuating photon intensity profile[18] which comprises of tunable optical parameters like absorption and scattering coefficients derived from independent[19] single Mie scattering theory to find the temperature rise in the tissues. Biological systems contain diverse chemical components associated with large water content. Several studies[20, 21] have been carried out by assuming these components as particles and analyzing the interaction of light with tissue in terms of light propagation in particulate media. We consider such a particulate medium and suppose that the photon intensity attenuates due to absorption with depth and as it is susceptible to Rayleigh scattering and most of the photons pass scattered but remains in the system. As the photons travel deeper, during the course of their propagation, they experience several collisions, termed as multiple scattering (Fig. 3(a)) due to backscattering and forward scattering, leading to heat generation at depth. Collimated laser beams

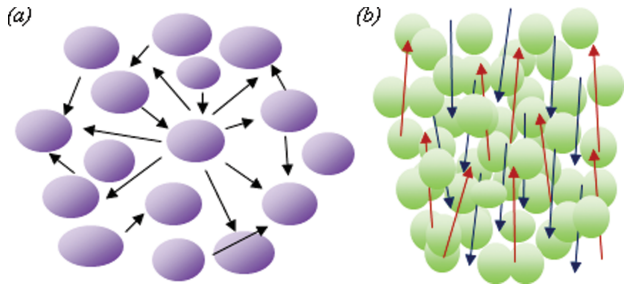

Figure 3. (a) Multiple scattering and absorption observed by the particles in the system. The black arrows represent the scattered/incident photon from/on the particle. The particles get radiation contribution from photons coming from all directions both by direct irradiation and scattered components. The scattered photons loss energy but contributes continuously by subsequent absorption by new absorption sites. (b) The forward and backward scattering shown schematically, the blue arrows show the forward scattering and the red arrows imply the coherent backscattering experienced by the laser beam.

specifically undergo coherent backscattering[22] by restricting spread in the beam path, causing enhanced absorption inside the tissue (Fig. 3(b)). We model this phenomenon as follows. Assuming light distribution inside the axisymmetric tissue is due to a Gaussian beam whose intensity at depth z and at radius r from centerline of the beam is given by,

$$I(r,z) = I_0 \exp\left\{-\frac{r^2}{[2\sigma^2(z)]}\right\}\{\exp(-\alpha z)\} \times \{1-\exp(-\beta z)\} \quad (1)$$

Here I is the light intensity at a given location (r, z). I_o is the intensity at the location (0, 0). The first, second and third exponential terms in Eq. (1) account for of the Gaussian profile of the laser beam, the attenuation of beam due to absorption and the re-enhancement of photon density at a distance z due to multiple scattering, respectively. The last two terms compete to result in the peak photon intensity at a particular depth which is a function of absorption coefficient (α) and scattering coefficient (β). Equation (2) considers the effect of beam broadening,

$$\sigma^2(z) = \sigma^2(0)\exp(\beta z) \quad (2)$$

Hence Eq. (3) gives the heat generation term,

$$Q(r,z) = \alpha I(r,z) = \alpha I_0 \exp\left\{-\frac{r^2}{[2\sigma^2(0)\exp(\beta z)]}\right\} \times \{\exp(-\alpha z)\}\{1-\exp(-\beta z)\} \quad (3)$$

In the following simulation, $I_o = 3.5 \times 10^4$ W/m^2 (corresponding to laser power 446 mW), beam radius at (0, 0) $\sigma(0)$ was 2 mm, $\beta = 530$ m^{-1} (for with and without nanoparticle case), $\alpha = 40$ m^{-1} (without nanoparticle) and 300 m^{-1} (with nanoparticle).[5]

Heat Transfer Analysis of the Model Tissue

The cylindrical axisymmetric shaped biomaterial in the test beaker is the computational domain. The transient heat transfer equation (Eq. (4)) Was solved in this domain with the heat generation term given in Eq. (3).

$$\rho C_p \frac{\partial T}{\partial t} + \nabla(-k\nabla T) = Q(r, z) \qquad (4)$$

The computation was carried out using the finite element software COMSOL™ Multiphysics. The bottom and side boundaries were enclosed in fused silica (beaker material), the outside being convective condition with ambient temperature of 28 °C convection boundary condition of 20 W/m^2 K. The top surface was subjected to a convection boundary condition of 20 W/m^2 K and ambient temperature of 28 °C. The initial temperature of gel is 28 °C. The thermal properties were as follows. For collagen gel the following properties were used. Mass density (ρ) = 1050 Kg/m^3; specific heat (C_p) = 3700 J/Kg K; thermal conductivity (k) = 0.5 W/m K[5]. For fuse silica, the default values of the software were used. A mesh independence study was performed to optimize number of mesh elements with reasonable amount of solution time.

RESULTS

Observation of Enhanced Temperature Inside Tissue Mimics

Transient response of all the thermocouples was taken by irradiating the biomaterial gel with laser at different powers. The temperature variation with depth and transient evolution of temperature are demonstrated in Figures 4 and S-5, respectively. Both the plots show that the temperature increases with depth up to a certain distance and then decreases gradually. Such initial increase in temperature is unusual which to the best of our knowledge is not reported earlier. The observations agree well with the experiments using agar gel (Figs. S-6 and S-7). According to Beer-Lambert law, there should be an attenuation of photon intensity from the tissue mimic surface and consequently temperature should decrease if there is no heat source inside. In any semitransparent system this is the expected consequence of light propagation. With increasing power, the temperature rise is enhanced but the temperature peak is at the same depth. In the case of collagen gel irradiation (cf Fig. 4) the maximum temperature rise is at 1 cm depth whereas considerable temperature rise occurs at 1.5 cm depth as well. For real *in vivo* system, this temperature rise is expected to be observed in muscles beyond the skin leading to unanticipated tissue damage.

Potential of Nanoparticles to Restrict Damage Spatially in Tissue Mimics

In the next level of study, nanoparticle embedded tissues were subjected to the same experiment. The synthesized

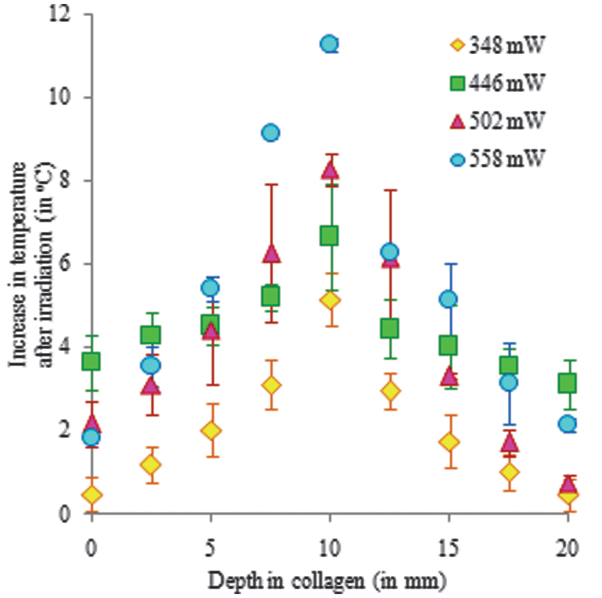

Figure 4. For pure collagen gel the temperature after 380 sec clearly increases inside the tissue up to certain distance and then decreases for all the power levels at all power levels. The maximum temperature increase can be observed at a distance of 10 mm from the surface. The power levels were 348 mW (pd = 2.77 W/cm^2), 446 mW (pd = 3.55 W/cm^2), 502 mW (pd = 3.99 W/cm^2) and 558 mW (pd = 4.44 W/cm^2).

nanoparticles were characterized for their optical properties. From spectrometric analysis, it was found that for gold mesoflowers, highest absorption occurs at 1100 nm, near to 1064 nm laser source used and gold nanospheres (cf Fig. 2) having an absorption peak at 690 nm, far away from the laser wavelength. These samples with nanoparticles yield even more surprising results. The temperature rise was not only enhanced in the presence of nanoparticles, but also the peak was shifted further towards the surface of the biomaterial. A steeper decreasing temperature profile was observed after the peak. Mesoflower resulted in higher temperature rise as the absorbance of mesoflower is higher at the operating wavelength of the laser (Fig. 5) for the same concentration of nanoparticle and the same power of the laser source. The temperature rise in the gold nanosphere embedded collagen case is less which can be explained by the decreased absorbance of the nanospheres at the operating wavelength of 1064 nm.

We performed the experiments for both types of nanoparticles for varying concentrations. With increasing concentration, the temperature rise was enhanced and the peak shifted towards the surface as well (Figs. 6 and 7). The temperature rise inside the tissue is not caused by nanoparticle aggregates because the nanoparticles were uniformly dispersed in the biomaterial by homogeneous mixing during sample preparation. This can be further confirmed from that fact that with smaller nanoparticle density the temperature peak is at deeper section and with higher nanoparticle density the temperature peak is closer to surface.

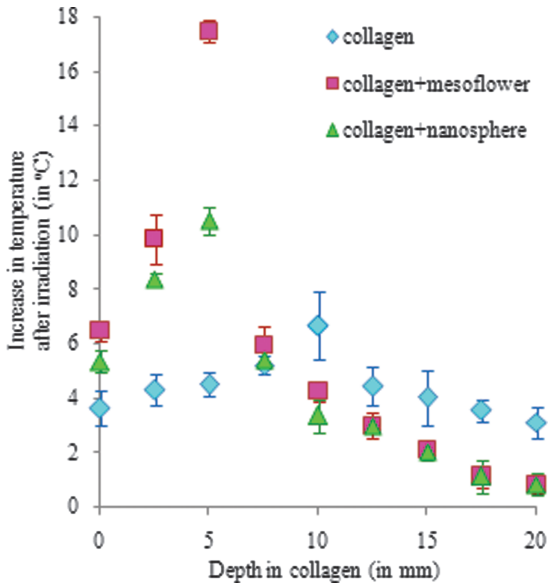

Figure 5. **Temperature distribution in the collagen gel after 380 sec for different system of tissue mimics at 446 mW (pd = 3.55 W/cm^2) power. The same trend of thermal profile is observed. The temperature rise is now much higher and the maximum temperature rise is restricted near the surface in presence of nanoparticles. Mesoflower results in higher temperature rise than nanosphere as at the operating laser wavelength, the mesoflower has higher absorbance.**

This is visible both with nanosphere and mesoflower (Figs. 6 and 7). If they were aggregated at a given section, we could see temperature rise only at that given section irrespective of nanoparticle concentration. From the experimental results we can summarize that, NIR irradiation

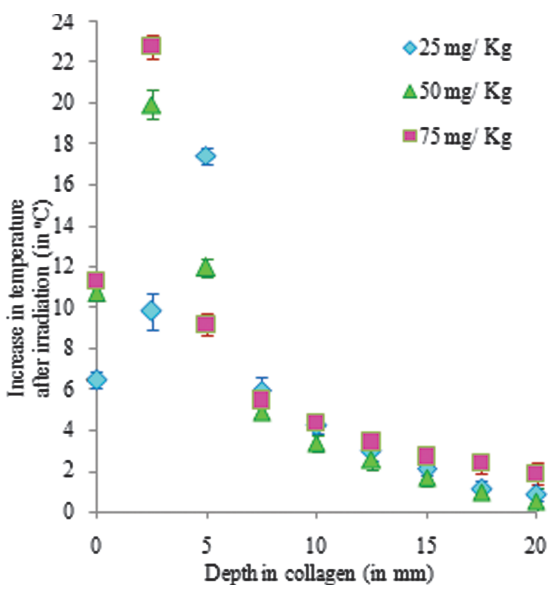

Figure 6. **With gold mesoflower concentration increasing the temperature increases inside but the peak shifts towards the surface and the temperature rise is restricted to a smaller depth (Experiment done at 446 mW, pd = 3.55 W/cm^2 power).**

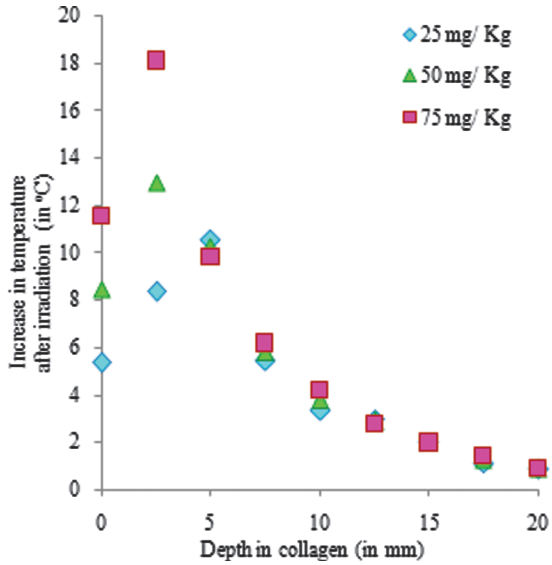

Figure 7. **The same trend similar to Figure 6 is observed for gold nanosphere as well (Experiment done at 446 mW power, pd = 3.55 W/cm^2).**

heats tissue to higher temperature at the subsurface than at the surface in contrast to expectation. Further the nanoparticles can restrict the temperature rise spatially. This anomalous thermal behavior of these tissue mimics is addressed next.

Collagen Microstructure Shows Higher Fiber Level Damage for Tissue Sample at Maximum Temperature

Figure 8 shows the AFM images of collagen microstructure. For both the cases of bare collagen and with nanoparticle it is visible that the tissue damage is more for deep tissue (7b, 7e, 7h), where the temperature is maximum compared to the surface (7a, 7d, 7g). After the maximum temperature is reached at further distances the temperature rise decreases resulting in less denaturated collagen structure (7c, 7f, 7i). The denatured collagen is characterized by breakage in collagen fiber. At lower temperature, the fibers maintain their morphology. As the temperature goes up the fibers start getting broken shown here as indentations.

Simulation of Thermal Profile in the Tissue Mimic

Figure 9(a) shows the peak heat generation intensity at depth according to the proposed model (Eq. (3)) whereas Figure 9(b) shows the steeply attenuating profile for the same values of α and β. This increased light induced heat generation may be the reason of enhanced temperature inside the biomaterial. Figure 10 shows the temperature rise in biomaterial found by simulation. For same power level, in pure collagen and mesoflower embedded collagen gels, the temperature increases up to a certain depth

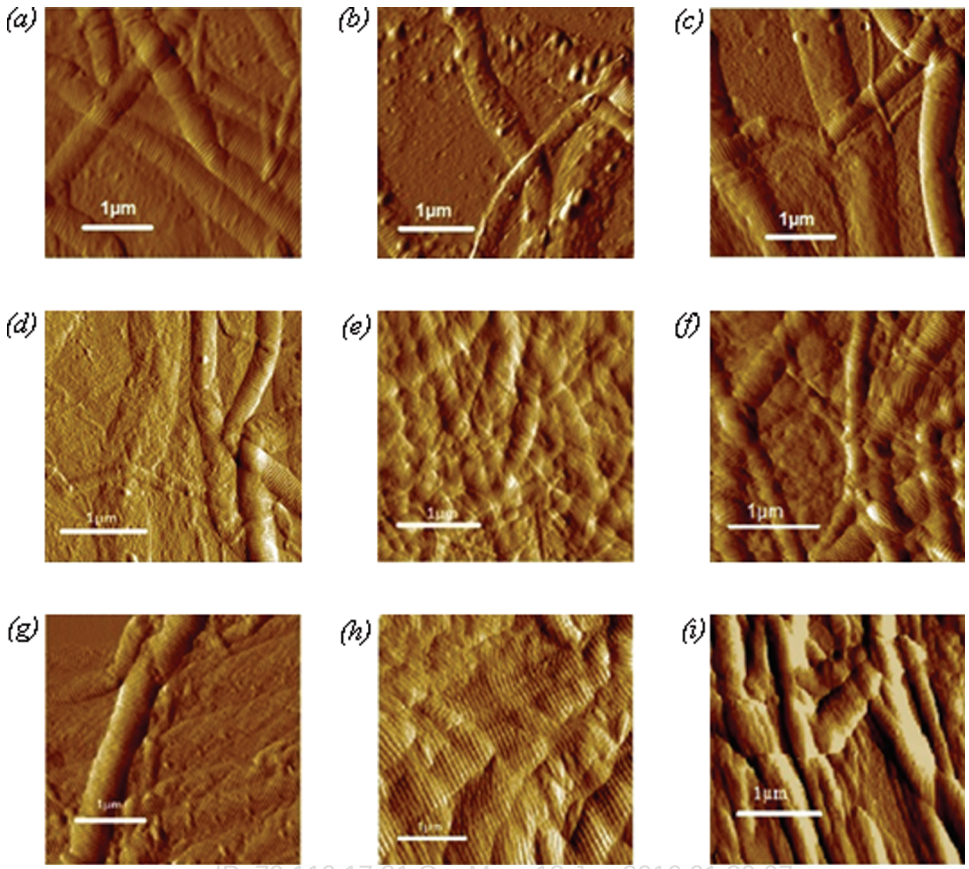

Figure 8. **Collagen microstructure at different depths. Pure collagen 446 mW (pd = 3.55 W/cm²) (a)–(c), pure collagen 558 mW (pd = 4.44 W/cm²) (d)–(f), collagen + mesoflower 558 mW (pd = 4.44 W/cm²) (g)–(i). At surface (a), (d), (g), at depth cporresponding to maximum temperature (b), (e), (h), at 2 mm distance deeper from maximum temperature point (c), (f), (i). In each case from surface to maximum temperature depth, the collagen denturation increases, after that the denaturation decreases.**

from the surface and then it decreases, closely matching with the experiment. The computational model closely follows the peak found 'at depth.' The effect of nanoparticle is also very crucial. Multiple scattering induced temperature enhancement happens both with and without nanoparticle. The effect is prominent with the presence of nanoparticles as presence of nanostructure enhances the temperature inside. It increases the absorptivity to a very high degree leading to high fraction of scattered light finally converted to heat, by restricting the photons near the surface.

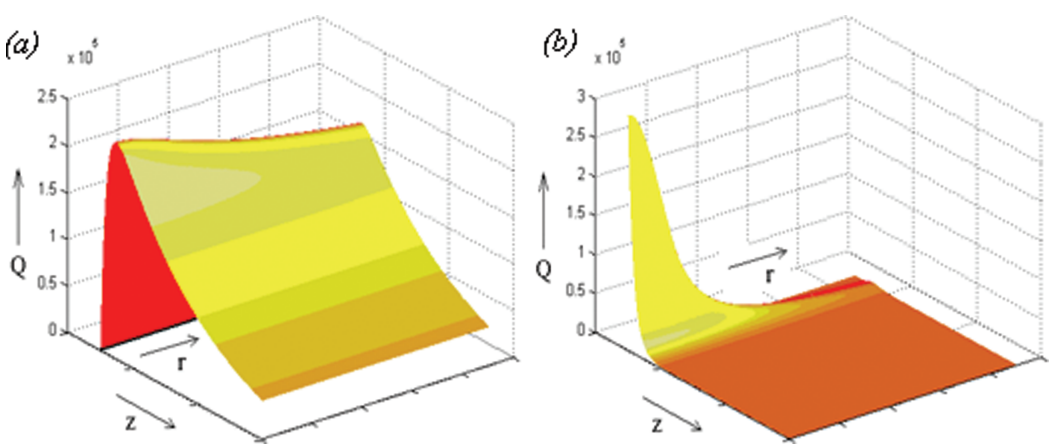

Figure 9. **The heat generation term $Q(r, z)$. (a) Our model proposes a heat generation peak deep inside the tissue; (b) The existing model proposes an attenuating heat generation profile.**

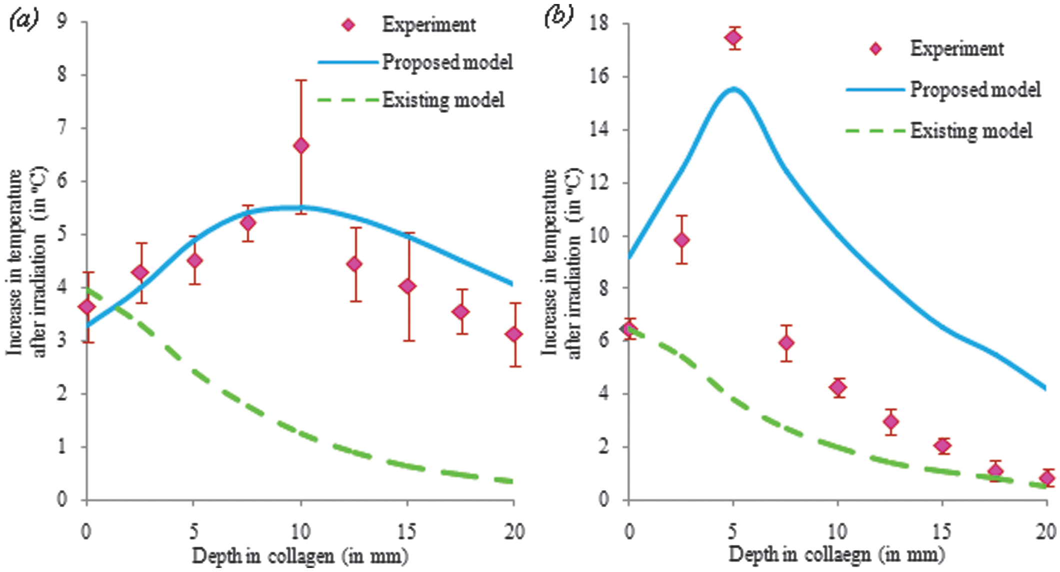

Figure 10. Temperature variation with depth with and without nanoparticle at constant power (Experimental and simulation) after 380 sec. (a) collagen gel, 446 mW (pd = 3.55 W/cm^2) (b) collagen gel + mesoflower at concentration of 25 mg/Kg, 446 mW (pd = 3.55 W/cm^2). Our proposed model closely resembles the experimental data for both the cases. The existing attenuating model severely underestimates the temperature inside tissue.

DISCUSSION AND CONCLUSION

The thermal damage due the spatiotemporal temperature history of tissue is an important issue. The most practiced quantification of thermal damage is given by Arrhenius type damage integral estimation;[23] essentially they use the temperature history estimated from models based on surface temperature measurement. The existing theory and models inherently lead to an attenuating temperature profile inside the tissue which predict an estimated damage and propose a corresponding therapeutic protocol which does not guarantee the aimed therapeutic outcome.

Near infrared light penetration depth is a few millimeter in the most transparent tissue.[24] For mammary carcinoma the penetration depth is 4.23 mm. From this work it can be seen that the highest temperature is recorded at 10 mm depth (bare biomaterial) and 5 mm (with nanoparticle), which clearly shows that even if the light does not penetrate this far, temperature rise occurs at considerable depth. The insight gained from this work proposes that NIR penetration leads to enhanced damages beyond the skin, i.e., in the muscle, having diverse consequences. The increased subsurface temperature attracts serious attention of photothermal therapists as the resulting tissue damage is severely underestimated in existing methods. The increased temperature inside tissue finally leads to increased damage of tissue at depth. This is a new understanding from our results. A practitioner based on the attenuating temperature model uses a particular dosage of the nanoparticle, laser power and other parameters. Underestimation of temperature may severely harm the healthy tissues. The tumor is actually heated to a much higher temperature along with the healthy tissues causing damage to it during therapy and afterwards due to thermal diffusion. Our findings should trigger further research in performing deep tissue temperature measurement experiments in more complex systems like viability of cells embedded in collagen gel, *in vivo* systems and finally to clinical settings. It should be further investigated what is the effect of other frequency range of EM spectrum in terms of temperature and microstructural change. Experiments should also be carried out with smaller size nanoparticles with size less than 100 nm which are of clinical relevance because of enhanced permeability and retention effect.[25] Still as the nanoparticles for photothermal therapy are designed to show high absorbance in the laser wavelength in practice, similar results are anticipated.

In this context, it is noteworthy to refer to the work of Jaunich et al.[26] who reported enhanced temperature inside laser irradiated tissue, but they used a focused laser beam which is quite definitive to give a subsurface thermal enhancement because of the focusing effect, where the tissue acts as a lens. Our study uses a collimated laser source (beam divergence at 1064 nm is less than 4.5 mrad) which also gives an enhanced thermal profile inside tissue. A divergent beam on refraction in a denser medium will become less divergent or at most parallel but in no way it can be convergent. So the heat generation enhancement inside tissue is not because of lensing effect. Another work by Elliott et al.[27] also experimentally and theoretically computed temperature distribution inside biomaterial (agar gel). But in their work the experimental system was different where two sets of gels were used (pure agar on top and agar + nanoshell at bottom) and no microstructural damage was not characterized in the biomaterial. In our work,

collagen gel was the primary candidate which undergoes temperature sensitive denaturation and the microstructural damage was correlated to temperature rise.

The theoretical model developed to explain the spatial distribution of temperature can be immensely helpful for photothermal therapy by predicting the optimal temperature and damage in tumor as well as in healthy tissues. The theoretical model proposed here is a phenomenological model based on the physical aspect of light propagation. It should be noted that ample amount of research was performed to predict light propagation inside tissue. Out of several approaches; solution of radiation transfer equation, diffusion approximated reduced radiation transfer equation and Monte Carlo methods are extensively studied. But experimental and theoretical studies coupling the physics of radiation transfer and heat transfer are very limited. The equations proposed here should be carefully applied in reconciliation to the existing methods.

There may be an argument that the lower temperature near surface is caused by convection heat loss. We performed heat transfer calculations to enquire this issue. With existing model if the surface temperature has to be this low, the convection heat transfer coefficient must be of the order of 1000 W/m^2 K. But in natural convection the typical value for convection heat transfer coefficient is 20 W/m^2 K. So, such drastically less temperature at surface is not caused by natural convection.

The primary experimental model system used in this research was collagen gel. To further confirm the observation of temperature rise, agar was used as another biomaterial. Though collagen is a representative model system widely used for tissue engineering research, in actual tumor physiological condition, the optical and thermal properties are different from those of normal tissue. Considering higher thermal conductivity and higher mass density of tumor the heat diffusivity of tumor tissue $\alpha = k/\rho C_p$ is similar to that of normal tissue and so variation in thermal properties between tissues should not make much difference in heat transfer physics. While looking optical properties we have at similar wavelength, absorption coefficient of normal healthy tissue is 26 m^{-1} (healthy tissue adjacent to female breast carcinoma, 850 nm), whereas for tumor it is 50 m^{-1} (female breast carcinoma, 900 nm). The reduced scattering coefficient (defined based on scattering coefficient and anisotropy parameter) are 820 m^{-1} for healthy tissue (female breast normal tissue, 810 nm) and 1310 m^{-1} for tumor tissue (female breast carcinoma, 750 nm).[1] Overall both absorption and scattering coefficients are higher for tumor tissue with respect to normal tissue. According to the model we proposed these values will lead to higher temperature and higher spatial thermal damage in tumor compared to normal tissue.

To apply the model *in vivo* several things need to be considered. The multilayer structure of skin, presence of muscle should be taken care of. The variation in optical and thermal properties will lead to complex computational modeling. Anisotropy in the thermal and optical properties should also be addressed. Finally the blood perfusion *in vivo* should also be included in the computational modeling for predicting temperature. As blood perfusion takes away heat, the temperature computed in this work is overestimated. Supporting information is available on request from corresponding author or from the following link: https://dl.dropboxusercontent.com/u/44919933/Ghosh%20et%20al_2013_Journal%20of%20Biomedical%20Nanotechnology_anomalous%20subsurface.pdf

Acknowledgments: We would like to thank Geoff Von Maltzahn in Massachusetts Institute of Technology (currently in Flagship ventures) for introducing Sarit Kumar Das to the problem; Central Leather Research Laboratory, Chennai, India for supplying the collagen and Dr. Shamit Bakshi for providing us the laser.

REFERENCES

1. V. D. Tuan (ed.,) Biomedical Photonics Handbook, CRC Press, Boca Roton, FL (**2003**).
2. J. V. Frangioni, *In vivo* near-infrared fluorescence imaging. *Curr. Opin. Chem. Biol.* 7, 626 (**2003**).
3. X. Huang, I. H. El-Sayed, W. Qian, and M. A. El-Sayed, Cancer cell imaging and photothermal therapy in the near-infrared region by using gold nanorods. *J. Am. Chem. Soc.* 128, 2115 (**2006**).
4. D. P. O'Neal, L. R. Hirsch, N. J. Halas, J. D. Payne, and J. L. West, Photo-thermal tumor ablation in mice using near infrared-absorbing nanoparticles. *Cancer Letters* 209, 171 (**2004**).
5. G. V. Maltzahn, J. H. Park, A. Agarwal, N. K. Bandaru, S. K. Das, M. J. Sailor, and S. N. Bhatia, Computationally guided photothermal tumor therapy using long-circulating gold nanorod antennas. *Cancer Reserach* 69, 3892 (**2009**).
6. R. Elghanian, J. J. Storhoff, R. C. Mucic, R. L. Letsinger, and C. A. Mirkin, Selective colorimetric detection of polynucleotides based on the distance-dependent optical properties of gold nanoparticles. *Science* 277, 1078 (**1997**).
7. D. S. Grubisha, R. J. Lipert, H. Y. Park, J. D. Driskell, and M. D. Porter, Femtomolar detection of prostate-specific antigen: an immunoassay based on surface-enhanced Raman scattering and immunogold labels. *Anal. Chem.* 75, 5936 (**2003**).
8. J. B. Jackson, S. L. Westcott, L. R. Hirsch, J. L. West, and N. J. Halas, Controlling the surface enhanced Raman effect via the nanoshell geometry. *Appl. Phys. Lett.* 82, 257 (**2003**).
9. X. M. Qian, X. H. Peng, D. O. Ansari, Q. Y. Goen, G. J. Chen, D. M. Shin, L. Yang, A. N. Young, M. D. Wang, and S. M. Nie, *In-vivo* tumor targeting and spectroscopic detection with surface-enhanced Raman nanoparticle tags. *Nature Biotechnolgy* 26, 83 (**2008**).
10. L. R. Hirsch, R. J. Stafford, J. A. Bankson, S. R. Sershen, B. Rivera, R. E. Price, J. D. Hazle, N. J. Halas, and J. L. West, Nanoshell-mediated near-infrared thermal therapy of tumors under magnetic resonance guidance. *Proceedings of National Academy of Science* 100, 3549 (**2003**).
11. R. S. Norman, J. W. Stone, A. Gole, C. J. Murphy, and T. L. Sabo-Atwood, Targeted photothermal lysis of the pathogenic bacteria, Pseudomonas aeruginosa, with gold nanorods. *Nano Lett.* 8, 302 (**2008**).
12. P. Diagaradjane, A. Shetty, J. C. Wang, A. M. Elliott, J. Schwartz, S. Shentu, H. C. Park, A. Deorukhkar, R. J. Stafford, S. H. Cho, J. W. Tunnell, J. D. Hazl, and S. Krishnan, Modulation of *in vivo* tumor radiation response via gold nanoshell-mediated vascular-focused

hyperthermia: characterizing an integrated antihypoxic and localized vascular disrupting targeting strategy. *Nano Lett.* 8, 1492 **(2008)**.

13. Y. Feng, D. Fuentes, A. Hawkins, J. Bass, M. N. Rylander, A. Elliott, A. Shetty, R. J. Stafford, and J. T. Oden, Nanoshell-mediated laser surgery simulation for prostate cancer treatment. *Engineering with Computers* 25, 3 **(2009)**.

14. D. Dasgupta, G. V. Maltzahn, S. Ghosh, S. N. Bhatia, S. K. Das, and S. Chakraborty, Probing nanoantenna-directed photothermal destruction of tumors using noninvasive laser irradiation. *Appl. Phys. Lett.* 95, 233701 **(2009)**.

15. Y. Bayazitaglou. Nanoshell assisted cancer thermal therapy: Numerical simulations. *Proceedings of the ASME 2009 2nd Micro/Nanoscale Heat and Mass Transfer International Conference*, Shanghai, China **(2009)**.

16. P. R. Sajanlal and T. Pradeep, Mesoflowers: A new class of highly efficient surface-enhanced Raman active and infrared-absorbing materials. *Nano Research* 2, 306 **(2009)**.

17. P. R. Sajanlal, T. S. Sreeprasad, A. S. Nair, and T. Pradeep, Wires, plates, flowers, needles, and core–shells: Diverse nanostructures of gold using polyaniline templates. *Langmuir* 24, 4607 **(2008)**.

18. A. J. Welch, The thermal response of laser irradiated tissue. *IEEE Journal of Quantum Electronics* 20, 1471 **(1984)**.

19. P. K. Jain, S. L. Kyeong, I. H. El-Sayed, and M. A. El-Sayed, Calculated absorption and scattering properties of gold nanoparticles of different size, shape, and composition: Applications in biological imaging and biomedicine. *J. Phys. Chem. B* 110, 7238 **(2006)**.

20. A. Bowling and A. F. Palmer, The small mass assumption applied to the multibody dynamics of motor proteins. *Journal of Biomechanics* 42, 1218 **(2009)**.

21. B. Jones, Modelling carcinogenesis after radiotherapy using Poisson statistics: implications for IMRT, protons and ions. *Journal of Radiological Protection* 29, A143 **(2009)**.

22. E. Akkerman, P. E. Wolf, and R. Maynard, Coherent backscattering of light by disordered media: Analysis of the peak line shape. *Phys. Rev. Lett.* 56, 1471 **(1986)**.

23. A. R. Moritz and F. C. Henriques, Studies of thermal injury. *The American Journal of Pathology* 23, 695 **(1947)**.

24. S. Stolik, J. A. Delgado, A. Perez, and L. Anasagasti, Measurement of the penetration depths of red and near infrared light in human "*ex vivo*" tissues. *Journal of Photochemistry and Photobiology B: Biology* 57, 90 **(2000)**.

25. H. Maeda, J. Wu, T. Sawa, Y. Matsumura, and K. Hori, Tumor vascular permeability and the EPR effect in macromolecular therapeutics: A review. *J. Controlled Release* 65, 271 **(2000)**.

26. M. Jaunich, S. Raje, K. Kim, K. Mitra, and Z. Guo, Bio-heat transfer analysis during short pulse laser irradiation of tissues. *Int. J. Heat Mass Transfer* 51, 5511 **(2008)**.

27. A. M. Elliott, R. J. Stafford, J. Schwartz, J. Wang, A. M. Shetty, C. Bourgoyne, P. O′ Neal, and J. D. Hazle, Laser-induced thermal response and characterization of nanoparticles for cancer treatment using magnetic resonance thermal imaging. *Medical Physics* 34, 3102 **(2007)**.